

Model of energy spectrum parameters of ground level enhancement events in solar cycle 23

S.-S. Wu^{1,2}, G. Qin³

¹State Key Laboratory of Space Weather, National Space Science Center, Chinese Academy of Sciences, Beijing 100190, China

²College of Earth Sciences, University of Chinese Academy of Sciences, Beijing 100049, China

³School of Science, Harbin Institute of Technology, Shenzhen, 518055, China

Key Points:

- Study of GLE energy spectrum parameters with conditions of the corresponding solar events
- Using solar conditions to determine whether there is strong interplanetary shock acceleration
- Preliminary prediction model of energy spectrum of ground level enhancement events

Abstract

Mewaldt et al. 2012 fitted the observations of the ground level enhancement (GLE) events during solar cycle 23 to the double power-law equation to obtain the four energy spectra parameters, the normalization parameter C , low-energy power-law slope γ_1 , high-energy power-law slope γ_2 , and break energy E_0 . There are 16 GLEs from which we select 13 for study by excluding some events with complicated situation. We analyze the four parameters with conditions of the corresponding solar events. According to solar event conditions we divide the GLEs into two groups, one with strong acceleration by interplanetary (IP) shocks and another one without strong acceleration. By fitting the four parameters with solar event conditions we obtain models of the parameters for the two groups of GLEs separately. Therefore, we establish a model of energy spectrum of solar cycle 23 GLEs which may be used in prediction in the future.

1 Introduction

Ground level enhancement (GLE) events are large solar energetic particle (SEP) events in which GeV particles are able to reach the Earth's atmosphere and produce secondary particles with intensities above the background level that is produced by the galactic cosmic rays (GCRs) so that the counts of ground-based neutron monitors (NMs) are enhanced [e.g., Reames, 1999; Lopate, 2006]. There are many studies on GLEs which can cause serious space weather effects [e.g., Shea and Smart, 2012]. Particularly in the solar cycle 23, there were even more GLE studies than previous periods because of more spacecraft in orbit, including NASA's SAMPEX, ACE, STEREO and NOAA's GOES series, onboard which the instruments broadened the measurements of protons in energy ~ 0.1 to $\sim 500 - 700$ MeV [Mewaldt et al., 2012]. In addition, SOHO and WIND spacecraft provided important observations for GLE study in solar cycle 23, i.e., the Large Angle and Spectrometric Coronagraph (LASCO) [Brueckner et al., 1995] onboard SOHO to provide the coronal images [e.g., Gopalswamy et al., 2010] and the Radio and Plasma Wave (WAVES) experiment [Bougeret et al., 1995] onboard WIND to provide the GLE associated radio dynamic spectra in the decameter-hecometric (DH) wavelengths [e.g., Gopalswamy et al., 2010]. Furthermore, the mass and kinetic energy of CMEs can be provided by the CME brightness obtained from LASCO observations [e.g., Vourlidas et al., 2000; Subramanian and Vourlidas, 2007], so that one can determine the strength of shock driver. The frequency of DH type II bursts from WAVES reflects the distance between interplanetary (IP) shock and the Sun [e.g., Gopal-

swamy, 2006], so that higher starting frequency indicates that the shock starts to accelerate particles in a closer distance with stronger effects. It is also indicated that lower ending frequency shows that the shock accelerates until it moves farther into the IP space, which suggests a strong shock. Furthermore, the composition data from Solar Isotope Spectrometer (SIS) [Stone *et al.*, 1998] onboard ACE spacecraft can be used to determine the source of the SEPs. For example, if the Fe/O ratio is higher, the SEPs are considered from flare material instead of the shock acceleration from solar wind or coronal materials [e.g., Reames, 1999; Cane *et al.*, 2003, 2006].

Some research has been done to study the GLEs detected in solar cycle 23, some work focused on individual events separately [e.g., Bieber *et al.*, 2002, 2004, 2005, 2013; Grechnev *et al.*, 2008; McCracken *et al.*, 2008; Firoz *et al.*, 2012], but others systematically focused on the total GLEs [e.g., Reames, 2009; Gopalswamy *et al.*, 2010, 2012; Mewaldt *et al.*, 2012]. Gopalswamy *et al.* [2010] studied the flare and CME properties, they found that the median value of flares associated with those GLEs except GLE61 is X3.8, which is far greater than that of all flares of solar cycle 23. For GLE61, though the flare occurred behind the west limb and the associated flare value is not determined, there might have a large flare because the associated CME was exceptionally fast (2465 km/s in sky plane and 2712 km/s deprojected). Gopalswamy *et al.* [2010] also found that the average speed of GLE associated CMEs during solar cycle 23 was as large as 1916 km/s in the sky plane. Note that there was no CME observation for GLE58 when SOHO was temporarily disabled. What's more, they found that every GLE has DH type II bursts, which indicates strong shocks [Gopalswamy, 2006]. Gopalswamy *et al.* [2012] is the enhanced version of Gopalswamy *et al.* [2010], and they given more information about the GLE associated flares and CMEs in solar cycle 23. What's more, they discussed the height of CMEs at solar particle release (SPR) times in detail, which was compared with the work of Reames [2009].

Based on the extended measurements of energetic protons from spacecraft, Mewaldt *et al.* [2012] tested three spectral forms for fitting energy spectra of solar cycle 23 GLEs. They found that the GLEs are best fitted by the double power-law shape of Band *et al.* [1993] rather than the Bessel function shape of Ramaty [1979] and the power-law with exponential-tail shape of Ellison and Ramaty [1985]. The equation of the double power-law is given by:

$$dJ/dE = \begin{cases} C (E/E_{\text{MeV}})^{\gamma_1} \exp(-E/E_0) & \text{for } E \leq \Delta\gamma E_0 \\ C_1 (E/E_{\text{MeV}})^{\gamma_2} & \text{for } E \geq \Delta\gamma E_0, \end{cases} \quad (1)$$

where

$$\begin{aligned}\Delta\gamma &= \gamma_1 - \gamma_2, \\ C_1 &= C (\Delta\gamma E_0 / E_{\text{MeV}})^{\Delta\gamma} \exp(-\Delta\gamma), \\ E_{\text{MeV}} &= 1 \text{ MeV},\end{aligned}$$

where J is fluence, and E is kinetic energy per nucleon. It is noted that there are four parameters in the double power-law Equation (1), namely, normalization parameter C , low-energy power-law slope γ_1 , high-energy power-law slope γ_2 , and break energy E_0 . The double power-law is a piecewise function, and the demarcation point is $\Delta\gamma E_0$, which is called transition energy [e.g., *Mewaldt et al.*, 2012]. Since $E_0 \gg E_{\text{MeV}}$, C is approximately equal to the spectrum value at $E = E_{\text{MeV}}$. If the maximum energy of measurements is less than transition energy, the spectrum can be fitted just using the upper expression of Equation (1), which is the Ellison-Ramaty form. However, since there were spacecraft measurements of extended energy channels available, it is possible for one to determine which formula to be appropriate.

It is convenient to use the double power-law with the form in Equation (1) for the model of SEP energy spectra since there are only four parameters needed. *Mewaldt et al.* [2012] studied the fitted parameters, i.e., C , γ_1 , γ_2 , and E_0 , of the double power-law model by comparing the results from the 16 GLEs and 22 large non-GLE events during solar cycle 23. They found that γ_1 of GLEs is usually similar to that of typical large SEP events, while γ_2 of GLEs is harder than that of typical large SEP events. They also found that E_0 of GLEs is usually in the range of ~ 2 to 46 MeV.

In this paper we analyze the double power-law parameters of GLEs during the solar cycle 23 with conditions of the corresponding solar events to obtain models of the parameters, thus the energy spectra of GLEs can be provided which may be used for prediction. In section 2, we introduce some observation characteristics of the intensity time profile of various energy protons and make the data selection. In section 3, we show the classification of the selected GLEs. In section 4 we present the correlations of energy spectrum parameters with solar activity. In section 5, we obtain the statistical expressions of C , γ_1 , γ_2 and E_0 , with which we establish a prediction model of energy spectrum of GLEs. Finally, we present conclusions and discussions in section 6.

2 Observations and Data Selection

In a GLE event, large amount of energetic particles are accelerated near the solar surface or in the IP space, and they are consequently transported in the heliosphere. The energetic particles can be measured in 1 AU by several spacecraft simultaneously, such as ACE, GOES, SAMPEX and STEREO missions. In Figure 1, we show the intensity time profile of energetic particles for GLE58, the fourth GLE in the solar cycle 23, from the Electron, Proton, and Alpha Monitor (EPAM) [Gold *et al.*, 1998] on ACE and Energetic Particle Sensor (EPS) [Onsager *et al.*, 1996] on GOES-8. For GLE58, there was an X1.0 class flare eruption at 21:50 on August 24, 1998, and the measurements of high energy protons, such as the 1.41 ~ 115 MeV protons, had an impulsive enhancement after tens of minutes. When an IP shock arrives at 1 AU, there is another enhancement of proton fluxes, which is called energetic storm particle (ESP) event [e.g., Mewaldt *et al.*, 2012]. The ESP event can significantly increase the intensity of low energy protons, such as 0.15 to 25.7 MeV protons, with the peak intensity higher than that caused by a flare or a corona shock. However, ESP event usually has little influence on high energy protons, such as tens to hundreds MeV protons. In general, the CME originated near central meridian associates with strong ESP event. For example, with the small longitude, GLE58 and GLE59 had strong ESP events, while GLE60 and GLE61, which had large longitude, were hardly affected by the IP shock. The intensity time profile of energetic protons in 1 AU lasts at least two days for a GLE, during which if an IP shock, in addition to the GLE associated one, corresponding to an earlier solar eruption arrives at 1 AU, the intensity of protons would be influenced by the additional IP shock. For example, in Figure 2 for GLE55, the start time of the event is 11:49 on November 6, 1997, and the arrival of the first shock is at 22:02 on the same day, which was less than 12 hours later than the flare associated to the GLE55, thus we consider the shock is not corresponding to the solar event of GLE55. Figure 3 exhibits the proton intensity time profiles for GLE56 with the flare eruption at 13:31 on May 2, 1998, and the arrival of the corresponding IP shock at 17:00 on 3 May. In addition to the associated IP shock, there was a large forward-traveling wave arriving at 02:15 on 4 May indicated by the black vertical dashed line, which significantly affected the low energy proton fluxes, such as 0.15 MeV to 6 MeV. Thus the energy spectra of the GLE55 and GLE56 are influenced, which may be the reason why their break energy E_0 are much bigger than that of other GLEs. Figure 4 shows the proton intensity time profiles for GLE68 with a flare eruption at 09:38 on January 17, 2005 indicated by a red vertical dashed line, but without the event associated IP shock at 1 AU. However, it is

shown that about 2 hours before the solar flare associated with GLE68, an IP shock associated with a previous solar event arrived at 1 AU indicated by a blue vertical dashed line, and we can find that the low energy proton intensity time profiles are affected by previous events. It can be shown that all of the GLEs except GLE68 in solar cycle 23 had a corresponding IP shock at 1 AU. Therefore, the energy spectra of GLE55, GLE56, and GLE68 are not usual comparing to other GLEs in solar cycle 23, for simplicity purpose, we exclude the three GLEs for further analysis. The above flare onset time and class are from *Gopal-swamy et al.* [2012], and the shock and wave information can be found in web (http://www-ssg.sr.unh.edu/mag/ace/ACElists/obs_list.html#shocks).

Energy spectrum can be obtained by integrating the intensity time profile of energetic particles observed by spacecraft near the Earth. Figure 5 shows the energy spectrum of a typical GLE with the four energy spectrum parameters. Note that, the value of normalization parameter C does not affect the shape of spectrum, but it controls the level of energy spectrum. Low-energy slope γ_1 is always affected by the ESP event especially when the shock nose is nearly toward the Earth, because ESP event can significantly enhance the low energy proton fluxes. It is assumed that high-energy slope γ_2 can be influenced only by a very strong toward-Earth IP shock.

In this work, the four parameters of GLEs' energy spectra during solar cycle 23 are obtained by *Mewaldt et al.* [2012]. The location of the flares associated to these GLEs are from *Mewaldt et al.* [2012]. The longitude of the flares range from E09 to W117, and the asymmetry of longitude is caused by the transport of SEPs in the Parker spiral field. The above parameters for GLEs in solar cycle 23 are listed in Table 1. In this work we would analyze the four parameters depending on the event conditions for the 13 selected GLEs in solar cycle 23.

3 Classification of Events

Since strong IP shock acceleration of energetic particles for a GLE can enhance the low energy part of energy spectrum significantly, the high-energy power-law slope γ_2 would become smaller. Figure 6 shows γ_2 as a function of the flare longitude θ . The numbers in the figure indicate the GLE number. We set threshold values $\theta_t = W40$ and $\gamma_{2t} = -3.6$. The vertical dashed line, $\theta = \theta_t$ divides all events into two parts. We assume that $\theta \leq \theta_t$ and $\theta > \theta_t$ indicate the IP shock nose being nearly toward the Earth and not toward the Earth, re-

spectively. In addition, the horizontal dashed line, $\gamma_2 = \gamma_{2t}$, divides all events into two parts. We assume that $\gamma_2 \geq \gamma_{2t}$ and $\gamma_2 < \gamma_{2t}$ indicate strong and weak IP shock acceleration, respectively. We divide GLEs into two categories, green events with strong IP shock acceleration and blue events with weak IP shock acceleration. From the figure we can see that all the events with IP shocks being not toward the Earth have weak IP shock acceleration. However, if the IP shock nose is toward the Earth, the events could be either in green or blue category. We assume relatively a green event corresponds to stronger solar event. Therefore, it is possible we use other solar event conditions to distinguish between the green and blue events if the shock nose is toward the Earth.

Firstly, we can use the gray level of CME image to distinguish between the blue and green events if the shock nose is toward the Earth. The white light image of CME can be obtained from the LASCO onboard SOHO. The main steps are as follows. First, we select a sequence of images which recorded the evolution of a CME and a pre-event image from the LASCO/C2 field of view and convert them to gray images, then use the median filtering algorithm [e.g., *Shen and Qin*, 2016] to get the so called "clean" images by removing their noise. Next, we make differences of the clean images between the event time ones and the pre-event one to obtain the pure CME images. Last, for each of the pure CME images we calculate the average gray value, of which we choose the largest value to denote as the gray level ϕ of the event.

Figure 7(a) exhibits one of the CME images of GLE59, and Figure 7(b) shows the clean image by removing the noise in Figure 7(a), Figure 7(c) is the clean image at pre-event time, and Figure 7(d), which is called the pure CME image of GLE59, is obtained by subtracting Figure 7(c) from Figure 7(b). The white circle in the figure represents the size of the Sun, and the small red circle represents the size of the occulting disk of C2. The average gray value is calculated in the area between the two red circles. Figure 8 is similar as Figure 7 except that it is for GLE70. Comparing the pure CME images of GLE59 and GLE70 we can find that the CME gray level of GLE70 is significantly lower than that of GLE59. The gray level ϕ of the events with shock nose toward the Earth are plotted as function of γ_2 in Figure 9, and we find that ϕ of green events are larger than that of blue events. Note that GLE58, a green event, is not included in the Figure 7 since there was no C2 data available for GLE58. Furthermore, we can set the threshold value $\phi_t = 13$. When the longitude θ of a GLE is less than the threshold θ_t , γ_2 would be smaller and larger than γ_{2t} indicating the strong and weak IP shock acceleration if ϕ is larger and smaller than ϕ_t , respectively. The

gray level ϕ of events with shock nose toward the Earth are shown in Table 2, in which we show other parameters used about GLEs in solar cycle 23. LASCO/C3 field of view can also record the evolution of CME, so one can use C3 images to determine the IP shock acceleration strength similarly.

Next, we show that the starting and ending frequency of DH type II bursts from the WAVES onboard WIND data can also be used to separate the green and blue events if the shock nose is toward the Earth. In Figure 10 we show γ_2 as a function of the starting and ending frequency of the associated DH type II bursts, obtained by *Gopalswamy et al.* [2010], in left and right panels, respectively. It is noted that the maximum frequency measurements are 14 MHz, so the starting frequency of the green events are all greater than or equal to 14 MHz. We can find that both the starting and ending frequency of DH type II bursts are effective in distinguishing the blue and green events. The frequency of DH type II bursts reflects the distance between IP shock and the Sun [e.g., *Gopalswamy*, 2006], so that high starting frequency indicates that the shock starts to accelerate particles in a closer distance. Therefore, the green events with a closer distance to start accelerating may have stronger acceleration of the shock. The ending frequencies of the green events are less than that of the blue ones, it is suggested that the shocks of the green events are strong enough to accelerate particles in farther IP medium. However, in space weather prediction one may use the starting frequency, instead of the ending one, of DH type II bursts to distinguish the blue and green events.

Furthermore, the event-integrated Fe/O ratio and Ne/O ratio can be used to determine the acceleration source [e.g., *Reames*, 1999]. Figure 11 shows the 12–45 MeV/nuc Fe/O ratio, obtained by *Mewaldt et al.* [2012], from ACE/SIS measurements. It is shown that for $\theta < \theta_t$, if the 12–45 MeV/nuc Fe/O ratio is smaller (larger) than 0.15, γ_2 would be smaller (larger) than γ_{2t} , indicating strong (weak) IP shock acceleration. It is assumed that the high value of 12–45 MeV/nuc Fe/O ratio indicates the SEPs source from flare material, while the low value indicates the SEPs source from solar wind or coronal materials [e.g., *Reames*, 1999; *Cane et al.*, 2003, 2006]. The SEPs source from solar wind or coronal materials indicates stronger IP shock acceleration than SEPs source from flare materials does. We can get similar results with 12–45 MeV/nuc Ne/O ratio. From the above analysis, it is shown that the 12–45 MeV/nuc Fe/O ratio and Ne/O ratio can be used to determine if the IP shock acceleration strong or weak, the results are consistent with our previous findings. In addition, other properties such as ionization-state and isotope abundance studied by *Reames* [1999] may also

distinguish these events effectively. However, the composition data of an SEP event are too late for one to use for prediction of GLE spectra.

Therefore, one can use the gray level ϕ and the starting frequency of the DH type II bursts to distinguish between green and blue events if the shock nose is toward the Earth.

4 Correlations of Energy Spectrum Parameters with Solar Activity

GLEs are caused by solar eruptions, the strength of which is relevant to the solar activity. Thus, we assume that the energy spectrum is relevant to the solar activity. The 10.7 cm solar radio flux ($F_{10.7}$) is one of the indices of solar activity[e.g., *Tapping*, 2013], so that we can use $F_{10.7}$ to study the energy spectrum. Figure 12 shows the energy spectrum parameters, $\log E_0$, γ_1 , and γ_2 for the selected GLEs in solar cycle 23 in Panels (a), (b), and (c), respectively, as function of $F_{10.7}$ which is the value for previous day from the NOAA's Space Weather Prediction Center (SWPC, <ftp://ftp.swpc.noaa.gov/pub/warehouse>). Here, blue and green stand for blue and green events, respectively. Dashed lines indicate the linear fitting with r as the correlation coefficients. In Figure 12(a), E_0 increases with the increase of $F_{10.7}$ for both types of events, so that we assume that energetic particles may be accelerated more efficiently if the solar activity is high. In Figure 12(b), the sign of the slopes of the green and blue dashed fitting lines are opposite. In Figure 12(c), the green and blue dashed fitting lines have the same trend, while the green and blue lines are separated with the blue line is higher in the value of γ_2 since the strong IP shock acceleration can significantly increase the intensity of low energy particles to make high-energy slope γ_2 smaller.

Another energy spectrum parameter, the normalization parameter C , is not related to the shape of energy spectrum, but it controls the level of the energy spectrum, i.e., C is associated with the energy spectra in 1 MeV. It is known that the low energy protons can be influenced by the IP shock, whose strength is relevant with the flare longitude θ . Therefore, C is possibly relevant with θ . The strength of soft X-ray burst is also relevant with solar activity at the time of event [*Thomas and Teske*, 1971]. Therefore, C is assumed to be related to θ/F_{sxr} , where F_{sxr} is the integral soft X-ray flux of flare. Figure 12(d) exhibits the relationship between $\log C$ and θ/F_{sxr} which is obtained from the NOAA's SWPC (<ftp://ftp.swpc.noaa.gov/pub/warehouse>). Note that there is no data for F_{sxr} of GLE61 because it is a backside event, therefore we use the average of F_{sxr} of all other 15 events as

F_{sxr} of GLE61. From Figure 12(d) we can see that the sign of the slopes of the green and blue dashed fitting lines are opposite.

5 Energy Spectrum Model for GLEs

From the results in Figures 12, we may have the expressions of the four energy spectrum parameters for both blue and green events as follows:

$$C = 10^{a_1 \frac{\theta}{F_{sxr}} + b_1}, \quad (2)$$

$$\gamma_1 = a_2 F_{10.7} + b_2, \quad (3)$$

$$\gamma_2 = a_3 F_{10.7} + b_3, \quad (4)$$

$$E_0 = 10^{a_4 F_{10.7} + b_4}, \quad (5)$$

where the values of coefficients a_i and b_i ($i = 1, 2, 3, 4$) for both types of GLEs are listed in Table 3. The Equations (1) and (2)–(5) may be used to establish a model of energy spectrum with the flare's longitude θ , integral soft X-ray flux F_{sxr} , and 10.7 cm solar radio flux $F_{10.7}$ as the input. In addition, to determine the type of GLEs, gray level ϕ or the starting frequency of DH type II bursts of the events is also needed.

Now we compare the energy spectra between our new model and the spacecraft observations in solar cycle 23 in Figure 13. Here, δ indicates the disagreement between the model and the observations defined as the following:

$$\delta = \sqrt{\frac{1}{N} \sum_{i=1}^N [\log F(E_i) - \log f(E_i)]^2}, \quad (6)$$

where $F(E)$ and $f(E)$ are energy spectra from the model and observations, respectively. From upper left panel of Figure 13 we can see that δ of GLE57 is large because E_0 from model is not accurate relative to observation. It is also seen from Figures 12 that except E_0 , other parameters from the model for GLE57 are relatively accurate comparing to other events. On the other hand, from lower right panel of Figure 13 we can see that δ of GLE70 is less than that of GLE57 although in addition to a not accurate E_0 , its model also provides worse parameter γ_1 .

6 Conclusion and Discussion

In this paper, we analyze the four energy spectra parameters, i.e., the normalization parameter C , low-energy power-law slope γ_1 , high-energy power-law slope γ_2 , and break

energy E_0 , which are obtained from *Mewaldt et al.* [2012] by fitting the GLE observations during solar cycle 23 to the double power-law equation. In the statistics, we exclude GLE55, GLE56, and GLE68 out of the total of 16 GLEs in solar cycle 23 for simplicity purpose, because the conditions of the three GLEs are complicated comparing to that of the rest ones. We divide the selected GLEs into two types of events according to γ_2 , i.e., the blue and green events with large and small γ_2 , respectively. Because large enhancement of lower energy particles from strong IP shock acceleration would decrease γ_2 , we assume that the small γ_2 indicates strong IP shock acceleration. We find that all the events with large longitude θ are blue events with large γ_2 . But it is shown that with small longitude one need to distinguish between blue and green events. We find that the use of the gray level ϕ of CME, the starting and ending frequencies of DH type II bursts, and the 12–45 MeV/nuc Fe/O ratio and Ne/O ratio are different between the blue and green events, so that they can be used to distinguish the blue and green events. However, to consider about the availability of the data during near the solar eruption we may choose the gray level ϕ of CME or the starting frequency of DH type II bursts to distinguish the two types of events with small longitude.

We find in each type of GLE events, for the energy spectrum parameters, γ_1 , γ_2 , and E_0 are relevant with 10.7 cm solar radio flux, $F_{10.7}$, and C has strong correlation with the ratio between the longitude and the integral X-ray flux of the flare, θ/F_{sxr} . Therefore, we get expressions for the four parameters as function of solar event conditions in solar cycle 23, thus a model of energy spectrum for GLEs in the period is established. We also compare the energy spectra from model with the observed ones of solar cycle 23 GLEs. However, we can see that for the model there are cases with one inaccurate parameter resulting in very large error, but there are some other cases with several inaccurate parameters resulting small error because the effects of inaccuracy may offset each other.

The energy spectrum model we obtain may be helpful for the future prediction of the GLE's energy spectrum. One needs to get the inputs quickly enough after the solar eruption. In this model the value of $F_{10.7}$ of the previous day is used, thus the input for $F_{10.7}$ can be obtained on time. In addition, the flare longitude θ and F_{sxr} can be obtained quickly from the solar image observed by ground-based telescopes and soft X-ray flux observed by GOES Solar X-Ray Sensor (XRS) [*Hanser and Sellers*, 1996], respectively. If the longitude is small, we need the gray level ϕ from SOHO/LASCO/C2 or the starting frequency of DH type II bursts from WIND/WAVES to determine the type of an event. However, the gray level ϕ from SOHO/LASCO/C2 can not be obtained quickly for two reasons. Firstly, CME needs

thirteen minutes to one or two hours to transport to the view of C2. Secondly, the data of C2 are delivered to the Earth via Deep Space Network (DSN) stations if there is telemetry contact, but they have to wait for several hours otherwise (see the description about the very latest SOHO images, <https://sohowww.nascom.nasa.gov/data/realtime/image-description.html>). In addition, the data of radio bursts in DH wavelengths from WIND/WAVES are also delivered via DSN stations. Therefore, in order to use the energy spectrum model to predict one might have to wait as long as several hours after the solar eruption. It is important to study other physics parameters that can help to determine the strength of IP shock acceleration if we want to be able to determine the type of event quickly after the solar event.

In order to improve the model of GLE energy spectrum, among other efforts, we need to study the transport of GLEs by comparing the spacecraft observations with the numerical modeling [e.g., *Qin et al.*, 2011, 2013; *Wang et al.*, 2012; *Qi et al.*, 2017]. In addition, there are usually much more large non-GLE SEP events than GLEs in a solar cycle. Therefore, It is also essential for us to study the energy spectra for large non-GLE SEP events with the method similar to that in this work.

Acknowledgments

This work was supported in part by grants NNSFC 41574172, NNSFC 41374177, and NNSFC 41125016. We thank the *ACE* EPAM, SWEPAM, MAG, SIS; *GOES* EPS, XRS; *SOHO* LASCO; *WIND* WAVES teams for providing the data used in this paper. The *ACE* data are provided by the ACE Science Center and the *GOES* data by the NOAA. We appreciate the availability of the *WIND* data at the Coordinated Data Analysis Web. We also acknowledge the CDAW CME catalog which is generated and maintained at the CDAW Data Center by NASA and The Catholic University of America in cooperation with the Naval Research Laboratory. *SOHO* is a project of international cooperation between ESA and NASA.

References

- Band, D., J. Matteson, L. Ford, B. Schaefer, D. Palmer, B. Teegarden, T. Cline, M. Briggs, W. Paciesas, G. Pendleton, G. Fishman, C. Kouveliotou, C. Meegan, R. Wilson, and P. Lestrade (1993), BATSE observations of gamma-ray burst spectra. I. spectral diversity, *Astrophys. J.*, *413*, 281–292, doi:10.1086/172995.
- Bieber, J. W., W. Dröge, P. A. Evenson, R. Pyle, D. Ruffolo, U. Pinsook, P. Tooprakai, M. Rujiwarodom, T. Khumlumlert, and S. Krucker (2002), Energetic particle observations

- during the 2000 July 14 solar event, *Astrophys. J.*, *567*, 622–634, doi:10.1086/338246.
- Bieber, J. W., P. Evenson, W. Dröge, R. Pyle, D. Ruffolo, M. Rujiwarodom, P. Tooprakai, and T. Khumlumlert (2004), Spaceship Earth observations of the Easter 2001 solar particle event, *Astrophys. J.*, *601*, L103–L106, doi:10.1086/381801.
- Bieber, J. W., J. Clem, P. Evenson, R. Pyle, D. Ruffolo, and A. Sáiz (2005), Relativistic solar neutrons and protons on 28 October 2003, *Geophys. Res. Lett.*, *32*, L03S02, doi:10.1029/2004GL021492.
- Bieber, J. W., J. Clem, P. Evenson, R. Pyle, A. Sáiz, and D. Ruffolo (2013), Giant ground level enhancement of relativistic solar protons on 2005 January 20. I. Spaceship Earth observations, *Astrophys. J.*, *771*, 92, doi:10.1088/0004-637X/771/2/92.
- Bougeret, J.-L., M. L. Kaiser, P. J. Kellogg, R. Manning, K. Goetz, S. J. Monson, N. Monge, L. Friel, C. A. Meetre, C. Perche, L. Sitruk, and S. Hoang (1995), WAVES: The radio and plasma wave investigation on the Wind spacecraft, *Space Sci. Rev.*, *71*, 231–263, doi:10.1007/BF00751331.
- Brueckner, G. E., et al. (1995), The Large Angle Spectroscopic Coronagraph (LASCO), *Sol. Phys.*, *162*, 357–402, doi:10.1007/BF00733434.
- Cane, H. V., T. T. von Rosenvinge, C. M. S. Cohen, and R. A. Mewaldt (2003), Two components in major solar particle events, *Geophys. Res. Lett.*, *30*, 8017, doi:10.1029/2002GL016580.
- Cane, H. V., R. A. Mewaldt, C. M. S. Cohen, and T. T. von Rosenvinge (2006), Role of flares and shocks in determining solar energetic particle abundances, *J. Geophys. Res.*, *111*, A06S90, doi:10.1029/2005JA011071.
- Ellison, D. C., and R. Ramaty (1985), Shock acceleration of electrons and ions in solar flares, *Astrophys. J.*, *298*, 400–408, doi:10.1086/163623.
- Firoz, K. A., W. Q. Gan, Y.-J. Moon, and C. LI (2012), An interpretation of the possible mechanisms of two ground-level enhancement events, *Astrophys. J.*, *758*, 119, doi:10.1088/0004-637X/758/2/119.
- Gold, R. E., S. M. Krimigis, S. E. Hawkins III, D. K. Haggerty, D. A. Lohr, E. Fiore, T. P. Armstrong, G. Holland, and L. J. Lanzerotti (1998), Electron, proton, and alpha monitor on the Advanced Composition Explorer spacecraft, *Space Sci. Rev.*, *86*, 541–562, doi:10.1023/A:1005088115759.
- Gopalswamy, N. (2006) Coronal mass ejections and type II radio bursts, in *Solar Eruptions and Energetic Particles*, edited by N. Gopalswamy, R. A. Mewaldt and J. Torsti, p. 207–

- 220, American Geophysical Union, Washington, D. C.. doi:10.1029/165GM20.
- Gopalswamy, N., H. Xie, S. Yashiro, and I. Usoskin (2010), Ground level enhancement events of solar cycle 23, *Indian J. Radio Sp. Phys.*, *39*, 240–248.
- Gopalswamy, N., H. Xie, S. Yashiro, S. Akiyama, P. Mäkelä, and I. G. Usoskin (2012), Properties of ground level enhancement events and the associated solar eruptions during solar cycle 23, *Space Sci. Rev.*, *171*, 23–60, doi:10.1007/s11214-012-9890-4.
- Grechnev, V. V., et al. (2008), An extreme solar event of 20 January 2005: Properties of the flare and the origin of energetic particles, *Sol. Phys.*, *252*, 149–177, doi:10.1007/s11207-008-9245-1.
- Hanser, F. A., and F. B. Sellers (1996), Design and calibration of the GOES-8 solar x-ray sensor: The XRS, *Proc. SPIE*, *2812*, 344–352, doi:10.1117/12.254082.
- Lopate, C. (2006) Fifty years of ground level solar particle event observations, in *Solar Eruptions and Energetic Particles*, edited by N. Gopalswamy, R. A. Mewaldt and J. Torsti, p. 283–296, American Geophysical Union, Washington, D. C.. doi:10.1029/165GM27.
- McCracken, K. G., H. Moraal, and P. H. Stoker (2008), Investigation of the multiple-component structure of the 20 January 2005 cosmic ray ground level enhancement, *J. Geophys. Res.*, *113*, A12101, doi:10.1029/2007JA012829.
- Mewaldt, R. A., M. D. Looper, C. M. S. Cohen, D. K. Haggerty, A. W. Labrador, R. A. Leske, G. M. Mason, J. E. Mazur, and T. T. von Rosenvinge (2012), Energy spectra, composition, and other properties of ground-level events during solar cycle 23, *Space Sci. Rev.*, *171*, 97–120, doi:10.1007/s11214-012-9884-2.
- Onsager, T. G., R. Grubb, J. Kunches, L. Matheson, D. Speich, R. W. Zwickl, and H. Sauer (1996), Operational uses of the GOES energetic particle detectors, in *GOES-8 and Beyond*, edited by E. R. Washwell, *SPIE Conf. Proc.*, *2812*, 281, Society of Photo-Optical Instrumentation Engineers, Bellingham, Wash. doi:10.1117/12.254075.
- Qi, S.-Y., G. Qin, and Y. Wang (2017), Numerical simulations of solar energetic particle event timescales associated with ICMEs, *Res. Astron. Astrophys.*, *17*, 33, doi:10.1088/1674-4527/17/4/33.
- Qin, G., H.-Q. He, and M. Zhang (2011), An effect of perpendicular diffusion on the anisotropy of solar energetic particles from unconnected sources, *Astrophys. J.*, *738*, 28, doi:10.1088/0004-637X/738/1/28.
- Qin, G., Y. Wang, M. Zhang, and S. Dalla (2013), Transport of solar energetic particles accelerated by ICME shocks: Reproducing the reservoir phenomenon, *Astrophys. J.*, *766*,

- 74, doi:10.1088/0004-637X/766/2/74.
- Ramaty, R. (1979), Energetic particles in solar flares, in *Particle Acceleration Mechanisms in Astrophysics*, edited by J. Arons, C. Max, and C. McKee, p. 135–154, Am. Inst. of Phys., New York. doi:10.1063/1.32074.
- Reames, D. V. (1999), Particle acceleration at the sun and in the heliosphere, *Space Sci. Rev.*, *90*, 413–491, doi:10.1023/A:1005105831781.
- Reames, D. V. (2009), Solar release times of energetic particles in ground-level events, *Astrophys. J.*, *693*, 812–821, doi:10.1088/0004-637X/693/1/812.
- Shea, M. A., and D. F. Smart (2012), Space weather and the ground-level solar proton events of the 23rd solar cycle, *Space Sci. Rev.*, *171*, 161–188, doi:10.1007/s11214-012-9923-z.
- Shen, Z.-N., and G. Qin (2016), A study of cosmic ray flux based on the noise in raw CCD data from solar images, *J. Geophys. Res.*, *121*, 10,712–10,727, doi:10.1002/2016JA023376.
- Stone, E. C., et al. (1998), The solar isotope spectrometer for the advanced composition explorer, *Space Sci. Rev.*, *86*, 357–408, doi:10.1023/A:1005027929871.
- Subramanian, P., and A. Vourlidas (2007), Energetics of solar coronal mass ejections, *Astron. Astrophys.*, *467*, 685–693, doi:10.1051/0004-6361:20066770.
- Tapping, K. F. (2013), The 10.7 cm solar radio flux ($F_{10.7}$), *Sp. Weather*, *11*, 394–406, doi:10.1002/swe.20064.
- Thomas, R. J., and R. G. Teske (1971), Solar soft X-rays and solar activity II. soft X-ray emission during solar flares, *Sol. Phys.*, *16*, 431–453, doi:10.1007/BF00162486.
- Vourlidas, A., P. Subramanian, K. P. Dere, and R. a. Howard (2000), Large-angle spectrometric coronagraph measurements of the energetics of coronal mass ejections, *Astrophys. J.*, *534*, 456–467, doi:10.1086/308747.
- Wang, Y., G. Qin, and M. Zhang (2012), Effects of perpendicular diffusion on energetic particles accelerated by the interplanetary coronal mass ejection shock, *Astrophys. J.*, *752*, 37, doi:10.1088/0004-637X/752/1/37.

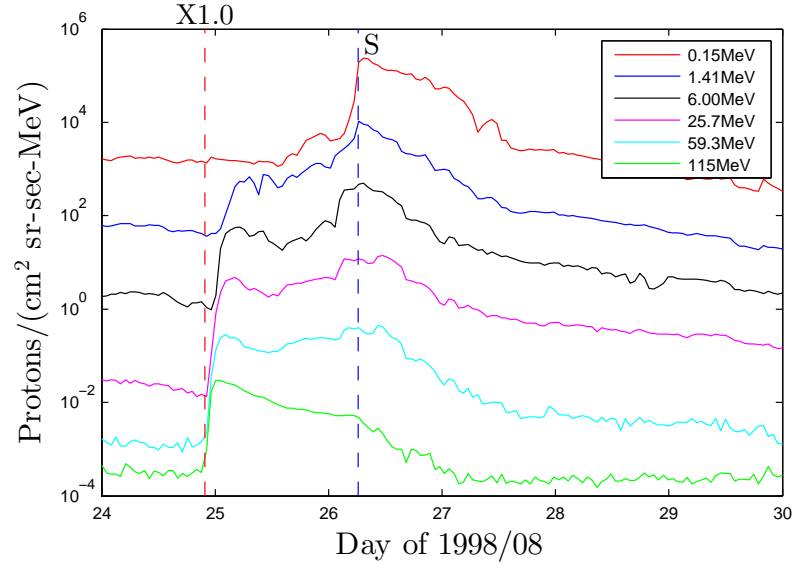


Figure 1. The time profile of energetic particles for GLE58. The orange and blue vertical dashed lines denote a solar flare eruption and an IP shock arrival, respectively.

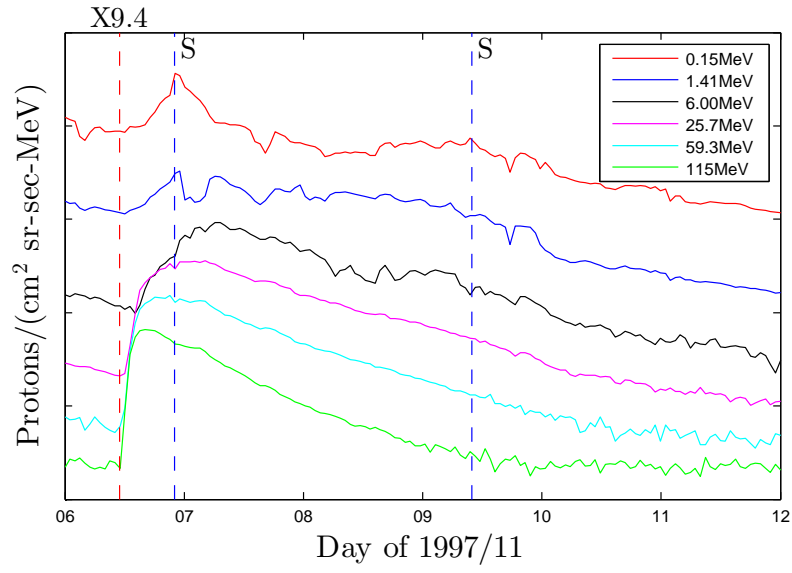


Figure 2. Similar as Figure 1 except for GLE55 and with two IP shocks.

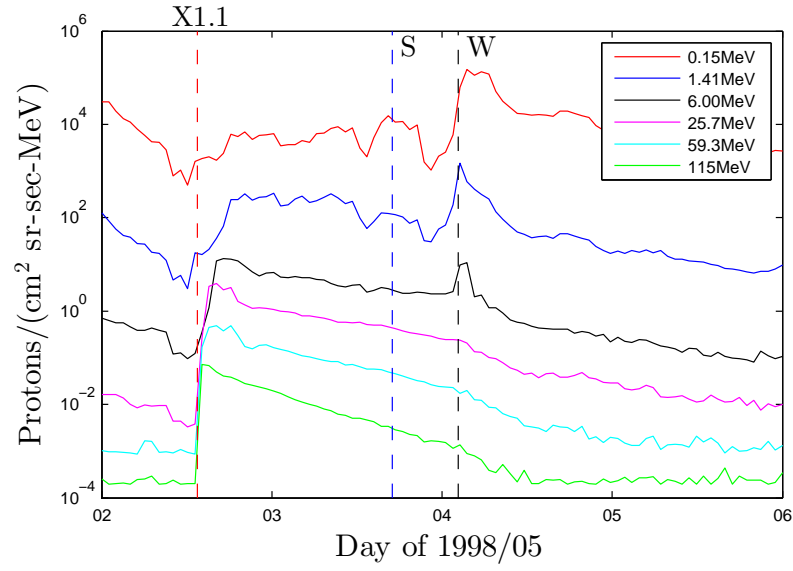


Figure 3. Similar as Figure 1 except for GLE56. The black vertical dashed line denotes the forward-traveling wave.

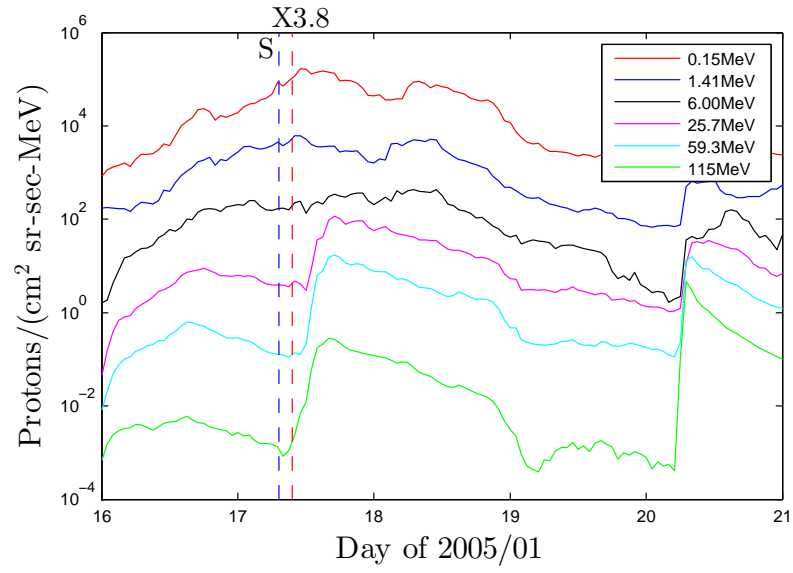


Figure 4. Similar as Figure 1 except for GLE68 and without event associated IP shock at 1 AU.

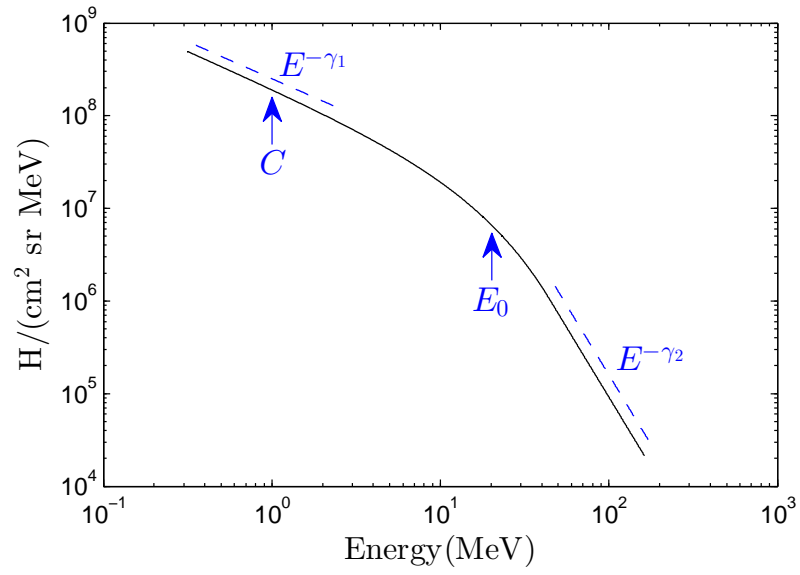


Figure 5. A typical double power-law energy spectrum with the four energy spectrum parameters.

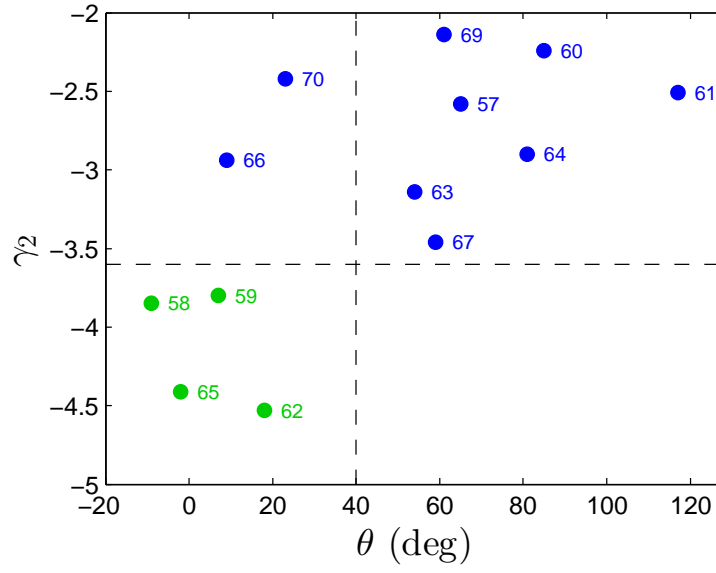


Figure 6. The high-energy slope γ_2 plotted versus flare longitude θ , and the numbers in the figure are the GLE number.

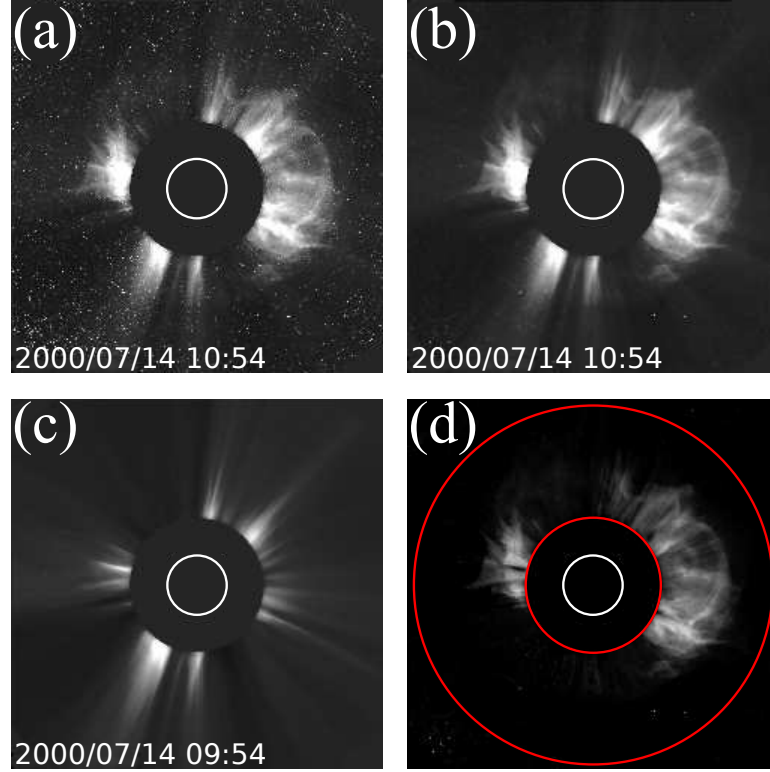


Figure 7. The CME images for GLE59. Panel (a) shows the CME image that has been converted to gray image observed by LASCO/C2 field of view; Panel (b) is similar as Panel (a) except that the noise is removed; Panel (c) shows the pre-event image with noise removed; Panel (d) shows the pure CME by making a difference between panel (b) and panel (c).

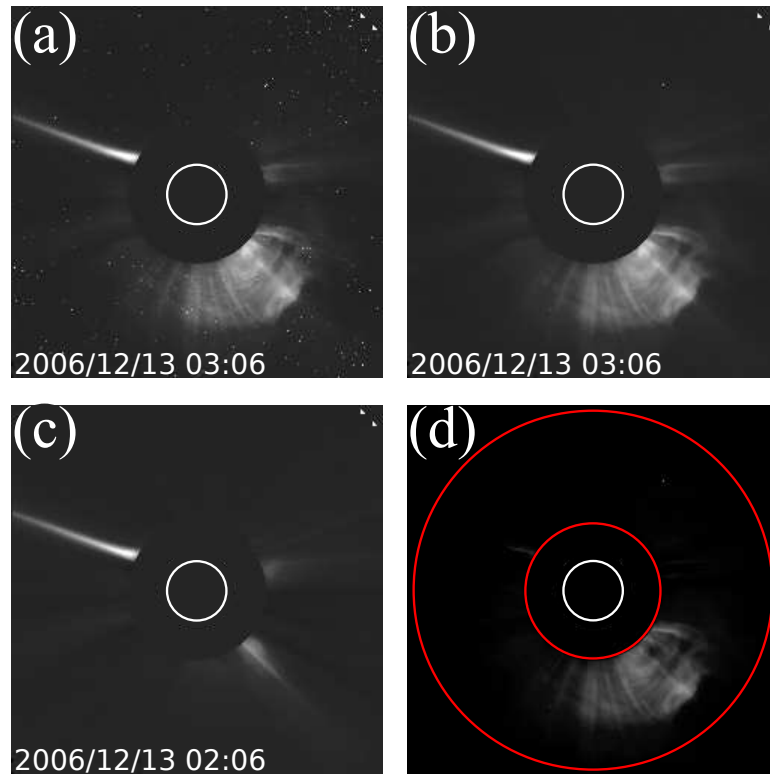


Figure 8. The same as Figure 7 except that the event is GLE70.

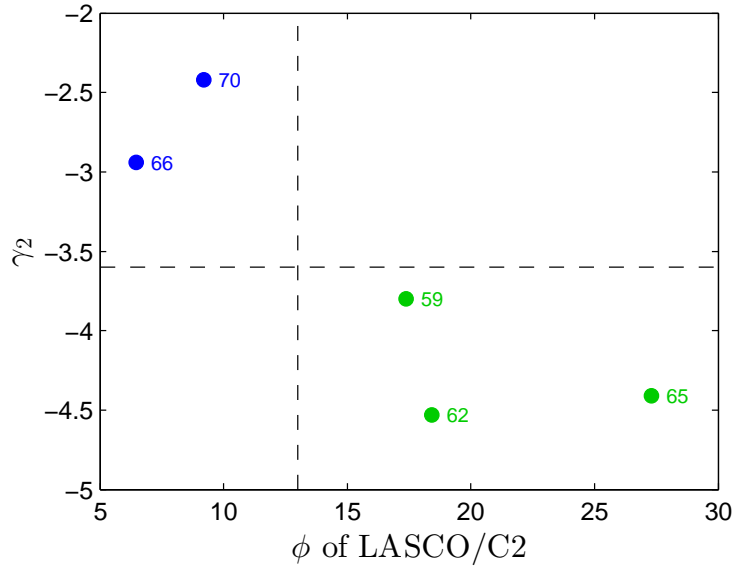


Figure 9. The high-energy spectrum slope γ_2 as a function of the gray level ϕ of the blue and green events with $\theta < \theta_l$.

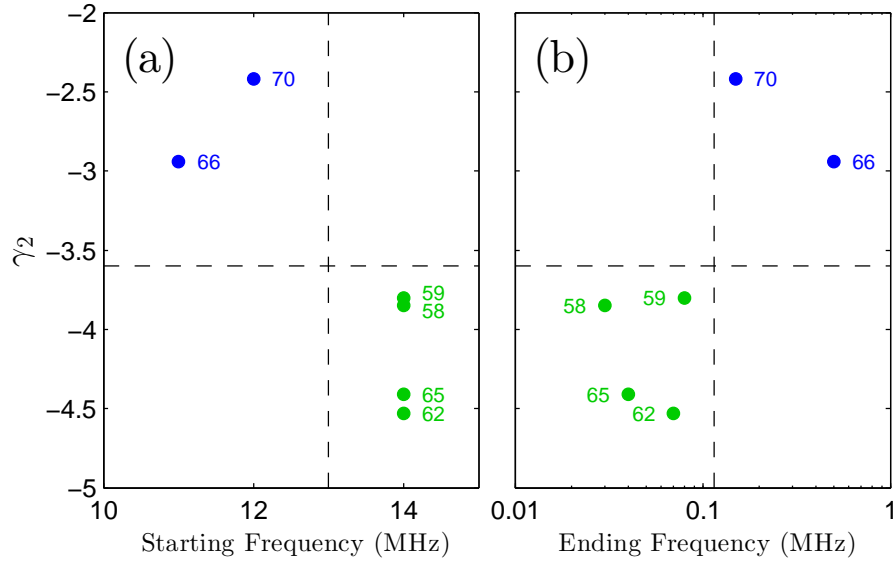


Figure 10. The high-energy spectrum slope γ_2 as a function of the starting and ending frequency of DH type II radio bursts in left and right panels, respectively, for blue and green events with $\theta < \theta_r$. Note that in panel (a) the starting frequencies of the green events are greater than or equal to 14 MHz.

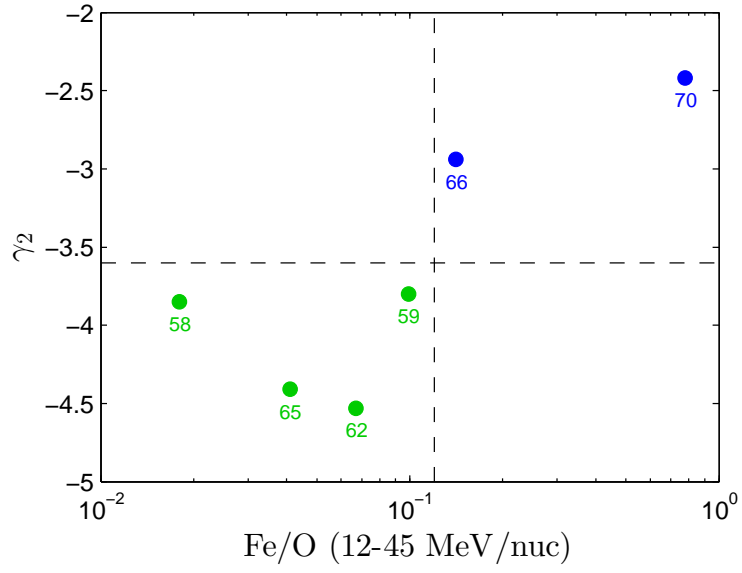


Figure 11. The high-energy spectrum slope γ_2 as a function of the 12–45 MeV/nuc Fe/O ratio measured by ACE/SIS for blue and green events with $\theta < \theta_t$.

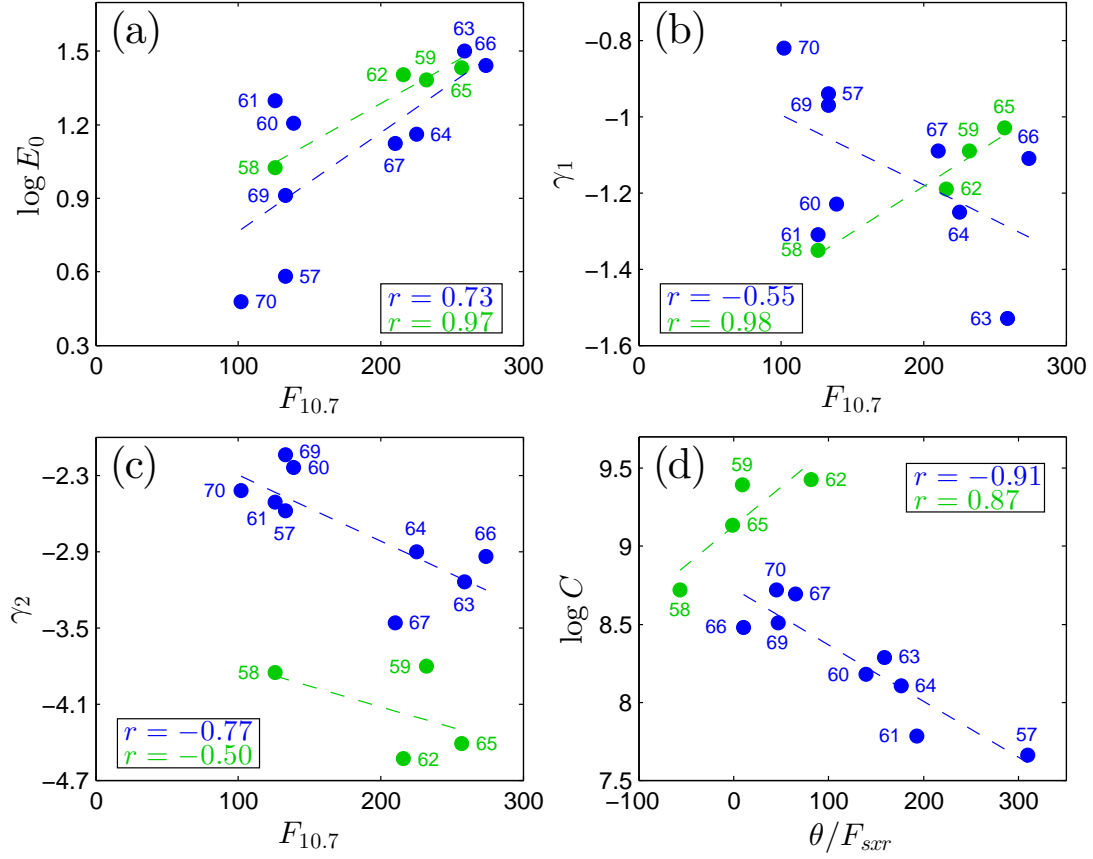


Figure 12. Three energy spectrum parameters, $\log E_0$, γ_1 , and γ_2 as function of the solar activity index $F_{10.7}$ in Panels (a), (b), and (c), respectively. Another parameter, $\log C$, is plotted as a function of θ/F_{srr} in Panel (d). Blue and green indicate the blue and green events, respectively. Dashed lines indicate the linear fitting with r as the correlation coefficient.

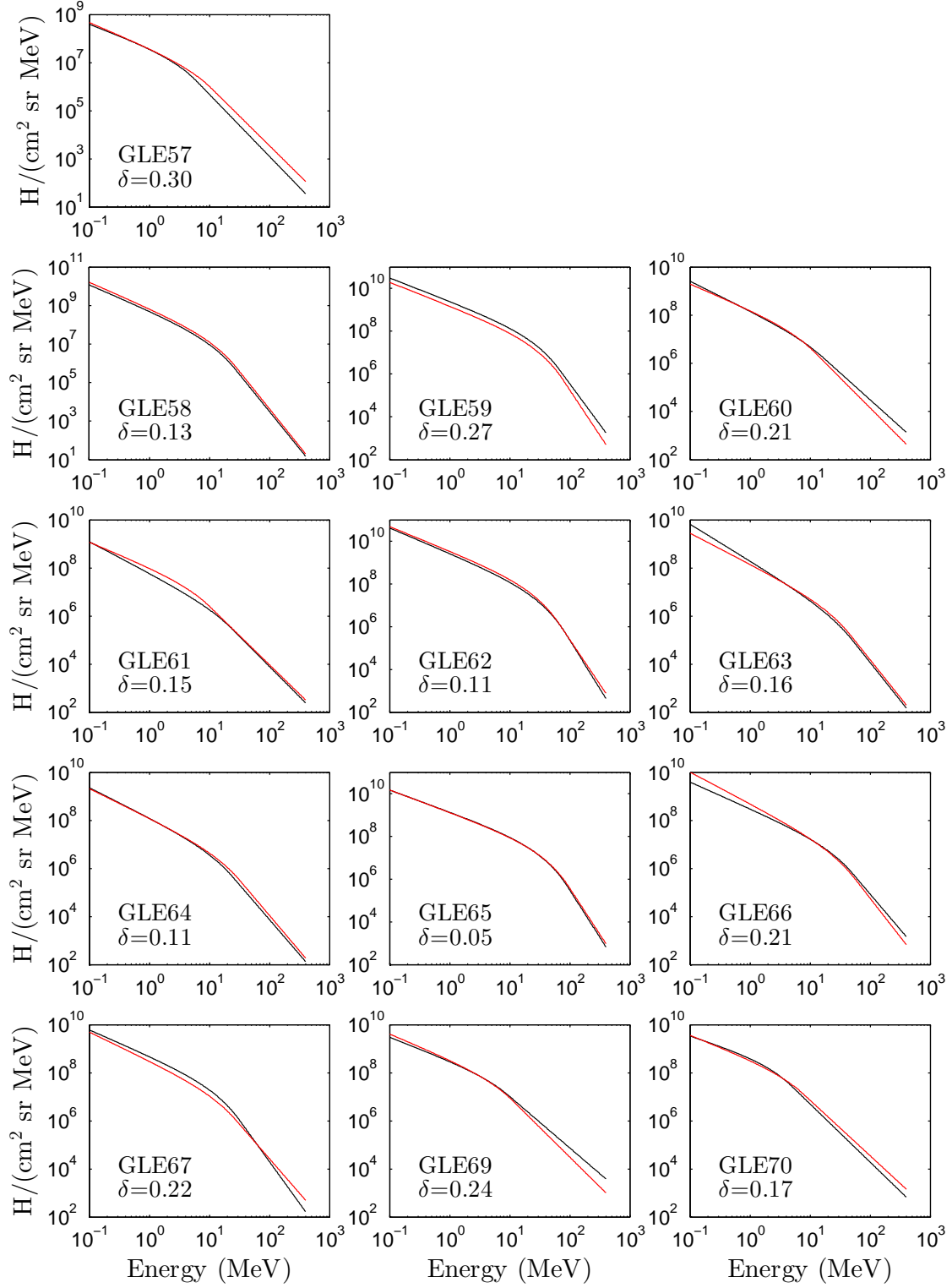


Figure 13. Energy spectra from observation and model in black and red, respectively, for 13 GLEs (number from 57 to 70 except for 68). δ is calculated with equation 6.

Table 1. Energy spectrum parameters, flare location and category of solar cycle 23 GLEs.

Event	Date	C	γ_1	γ_2	E_0	Location	Category
55 ^a	11/06/97	$1.28 \pm 0.07 \text{ E}+08$	-1.56 ± 0.03	-2.44 ± 0.14	91.3 ± 18.8	S18W63	
56 ^a	05/02/98	$4.49 \pm 0.30 \text{ E}+07$	-1.86 ± 0.02	-2.83 ± 0.20	$114. \pm 32.$	S15W15	
57	05/06/98	$4.59 \pm 0.86 \text{ E}+07$	-0.94 ± 0.14	-2.58 ± 0.08	3.81 ± 1.16	S11W65	blue
58	08/24/98	$5.27 \pm 0.49 \text{ E}+08$	-1.35 ± 0.05	-3.85 ± 0.11	10.6 ± 1.17	N35E09	green
59	07/14/00	$2.48 \pm 0.15 \text{ E}+09$	-1.09 ± 0.03	-3.80 ± 0.10	24.2 ± 1.9	N22W07	green
60	04/15/01	$1.51 \pm 0.16 \text{ E}+08$	-1.23 ± 0.07	-2.24 ± 0.04	16.1 ± 4.7	S20W85	blue
61	04/18/01	$6.05 \pm 0.62 \text{ E}+07$	-1.31 ± 0.07	-2.51 ± 0.05	19.9 ± 5.1	S23W117	blue
62	11/04/01	$2.68 \pm 0.17 \text{ E}+09$	-1.19 ± 0.03	-4.53 ± 0.11	25.4 ± 1.8	N06W18	green
63	12/26/01	$1.94 \pm 0.16 \text{ E}+08$	-1.53 ± 0.04	-3.14 ± 0.13	31.7 ± 5.5	N08W54	blue
64	08/24/02	$1.28 \pm 0.12 \text{ E}+08$	-1.25 ± 0.08	-2.90 ± 0.06	14.5 ± 2.8	S02W81	blue
65	10/28/03	$1.37 \pm 0.08 \text{ E}+09$	-1.03 ± 0.04	-4.41 ± 0.12	27.0 ± 2.1	S20E02	green
66	10/29/03	$3.03 \pm 0.17 \text{ E}+08$	-1.11 ± 0.05	-2.94 ± 0.13	27.7 ± 3.4	S19W09	blue
67	11/02/03	$4.94 \pm 0.31 \text{ E}+08$	-1.09 ± 0.05	-3.46 ± 0.12	13.3 ± 1.5	S18W59	blue
68 ^a	01/17/05	$7.37 \pm 0.48 \text{ E}+08$	-1.54 ± 0.04	-4.63 ± 0.15	40.5 ± 4.4	N14W25	
69	01/20/05	$3.22 \pm 0.34 \text{ E}+08$	-0.97 ± 0.11	-2.14 ± 0.06	8.18 ± 2.63	N14W61	blue
70	12/13/06	$5.25 \pm 0.85 \text{ E}+08$	-0.82 ± 0.10	-2.42 ± 0.03	3.01 ± 0.66	S06W23	blue

^a The events are excluded for statistical analysis.

Table 2. Some related parameters of solar cycle 23 GLEs.

Event	$\theta < \theta_t$	ϕ	f_{start} (MHz)	f_{end} (MHz)	Fe/O 12–45 MeV/n	F_{sxr} (W/m ²)	$F_{10.7}$ (sfu)
55 ^a	N					0.360 ^b	114
56 ^a	Y	04.31	5 ^c	3.00	0.683±0.016	0.067	113
57	N					0.210	133
58	Y		14	0.03	0.018±0.001	0.160	126
59	Y	17.39	14	0.08	0.099±0.010	0.750	232
60	N					0.610	139
61	N					0.606 ^d	126
62	Y	18.43	14	0.07	0.067±0.007	0.220	216
63	N					0.340	259
64	N					0.460	225
65	Y	27.30	14	0.04	0.041±0.004	1.800	257
66	Y	06.46	11	0.50	0.141±0.007	0.870	274
67	N					0.910	210
68 ^a	Y	10.02	14	0.03	0.031±0.001	0.840	145
69	N					1.300	133
70	Y	09.20	12	0.15	0.778±0.016	0.510	102

^a The events are excluded for statistical analysis.

^b 0.036 W/m² from SWPC, but we use 0.36 W/m² according to our calculation from GOES soft X-ray flux.

^c Earlier start possible $f_{start} = 14$ MHz at 14:06 hrs UT [Gopalswamy *et al.*, 2010].

^d No F_{sxr} for GLE61, we use the average of all other 15 GLEs.

Table 3. The values of coefficients a_i and b_i ($i = 1, 2, 3, 4$) of energy spectrum parameters for the two types of events.

i	Blue events		Green events	
	a_i	b_i	a_i	b_i
1	-0.003601	8.726740	0.005015	9.127913
2	-0.001842	-0.811214	0.002395	-1.662528
3	-0.005206	-1.777306	-0.003275	-3.467162
4	0.004038	0.360222	0.003259	0.634273